Solar Energy Materials & Solar Cells 230 (2021) 111190

Contents lists available at ScienceDirect

Solar Energy Materials and Solar Cells

journal homepage: www.elsevier.com/locate/solmat

Kinetics of silicon nitride coatings degradation and its influence on liquid infiltration in PV silicon crystallization processes

Rania Hendawi [a,*], Arjan Ciftja [b], Lars Arnberg [a], Marisa Di Sabatino [a]

[a] Department of Materials Science and Engineering, NTNU, 7491, Trondheim, Norway
[b] Ciftja Technologies AS, 7050, Trondheim, Norway

ARTICLE INFO

Keywords:
Coating
Depletion
Infiltration
Si_3N_4
Colloidal silica

ABSTRACT

Safe implementation of reusable crucibles in the silicon PV industry requires a thorough understanding of the reactions in the system to avoid liquid infiltration and crucible failure at high temperatures. Typically, an oxidized Si_3N_4-coating layer is applied to the crucibles to avoid wetting. During melting, the coating undergoes a transition in its wettability behavior as a result of oxide depletion. However, much uncertainty still exists about undergoing reactions and their effect on the coating depletion, and hence the wetting kinetics. Here we report on the coating's oxygen depletion mechanisms by applying a novel coating method to avoid conventional oxidation as it causes severe degradation of non-oxide crucibles. By adding colloidal silica to the silicon nitride coating, we (i) control the oxygen concentration in the coating, (ii) avoid the crucible degradation, and (iii) eliminate the pre-oxidation step. Furthermore, a quantification of the coating's oxygen content effect on the depletion rate was presented via an analytical model. These results provided insight into how the coating depletion can hinder the liquid infiltration by forming and stabilizing silicon oxynitride in the coating as evidenced by Raman mapping and thermodynamic calculations. The difference between the rates of liquid infiltration and oxygen depletion was also elucidated in detail.

1. Introduction

The vertical freeze gradient (VFG) casting remains an important technique in the silicon photovoltaic industry especially after the recent advances in quasi-mono Si that offers lower energy consumption and carbon footprint compared with the Czochralski method [1–6]. A further reduction in cost and waste can be achieved by replacing the single-use silica crucibles with reusable crucibles. Various attempts have been made to develop reusable crucibles for directional solidification applications [7–11]. Silicon nitride crucibles are the most promising due to their chemical stability, thermal durability and high purity [12]. Typically, the crucibles are coated with a high-purity silicon nitride layer that acts as a diffusion barrier and facilitates the ingot removal but liquid silicon partially wets silicon nitride coating [13]. Most studies have reported that oxidation of the coated crucibles can avoid silicon sticking or infiltration in the coating as silicon poorly wets SiO_2 that encapsulates Si_3N_4 particles [9–12]. Heating the coated crucibles for 2–4 h at 1100 °C in air is a common oxidation method in industry to introduce the oxide layer in the coating which in turn prevents wetting and infiltration.

Infiltration of any liquid in a porous solid is driven by two major factors: (i) viscous flow of the fluid into the pores - nonreactive infiltration; and/or (ii) reactive infiltration - a change in the chemical composition of the surface that is followed by a transition in the equilibrium contact angle [13]. The latter has been confirmed by most studies to be the main cause of the silicon spreading on the oxidized Si_3N_4-coating since the oxide products deplete during the process [11,14]. Some authors have studied the depletion (deoxidation) process of silicon nitride coating, in absence of liquid silicon, in vacuum and argon atmospheres [14,15]. They have claimed that the coating's depletion is mainly caused by the reaction of oxide products with silicon nitride at high temperatures. Huguet et al. [16] have suggested that the oxides deplete because they react with liquid silicon during melting, which indicates that deoxidation of the coating and infiltration of the liquid occur simultaneously. Based on this hypothesis, they have proposed a model to describe the liquid infiltration rate, but the model fails to demonstrate the infiltration behavior for coatings that oxidized at low temperature.

Until recently, little is known about the optimal oxygen content that is desirable to achieve non-wetting conditions. The research to date has claimed that the higher the oxidation level of the coating the better its

* Corresponding author.
E-mail address: rania.hendawi@ntnu.no (R. Hendawi).

https://doi.org/10.1016/j.solmat.2021.111190
Received 26 February 2021; Received in revised form 12 May 2021; Accepted 16 May 2021
Available online 3 June 2021

Table 1
Characteristics of Si_3N_4 powder.

Powder Characteristics	Value
α-Si_3N_4 content	>85%
Oxygen content	<1 wt%
Particle size	D98 < 7 μm
	D90 < 5 μm
	D50 < 2.2 μm

non-wetting properties. A crucial issue of the conventional oxidation method, besides being highly sensitive to the furnace and the coating conditions, is its incompatibility with non-oxide-base materials. Degradation of the silicon nitride crucibles during the conventional oxidation of the coating has been reported in a previous study [3]. A new coating and heat treatment need to be validated for the non-oxide materials such as silicon nitride by considering its influence on the wetting kinetics. Gong et al. [17] have been applied a mixture of nano-silica and silicon nitride coating on quartz substrates to enhance the binding strength and promote the permeation ability of the coating. However, no controlled studies have been reported the effect of silica addition on the wetting and coating degradation kinetics of non-oxide substrates. The first step in elucidating the wetting process is to understand the interactions in the Si-coating-crucible system and their effect on the coating degradation since much uncertainty still exists about the relation between the infiltration process and the coating degradation.

The current study aims to develop a suitable coating method for non-oxide crucibles such as Si_3N_4 crucibles. To achieve this, we have substituted the conventional oxidation method with a systemic addition of colloidal silica to the Si_3N_4-coating. This method has enabled us to: (i) better control the mass concentration of oxygen in the coating, (ii) determine the optimal oxygen content for the lowest wetting rate, and (iii) eliminate the pre-oxidation step which causes a severe degradation in silicon nitride crucibles. A thorough investigation of the coating depletion and the liquid infiltration has been also conducted in this work by in-situ melting of silicon on coated Si_3N_4-substrates followed by Raman mappings. Moreover, we have developed a model that describes the coating degradation kinetics in major regimes of the Si-coating-crucible system.

2. Experimental

A slurry composed of high purity Si_3N_4 powder and polyvinyl alcohol as a binder was dispersed in deionized water and sprayed by a 0.3 mm nozzle on the pre-heated reaction bonded silicon nitride (RBSN) substrates (10 × 10 × 5 mm^3) at 120 °C. The coating thickness was approximately 200–250 μm. The characteristics of Si_3N_4 powder are given in Table 1. We introduced oxygen to the coating by three different techniques:

(i) Oxidation of the coated substrates and crucibles at 1100 °C
(ii) Addition of colloidal silica to the coating slurry.
(iii) Pre-oxidation of the coating powder at 1100 °C

The last two methods were used to avoid conventional oxidation. However, The characteristics of RBSN are mentioned elsewhere [11]. The wetting experiments were performed in a sessile drop furnace. The furnace consists of a horizontal graphite heater surrounded by graphite radiation shields, located in a water-cooled vacuum chamber. The chamber was fitted with windows to allow a digital video camera (Sony XCD-SX910CR) to record the shape of the droplet during melting. To evaluate the wetting behavior, three main parameters were measured: i) the contact angle, ii) the height of the drop, and iii) the base diameter of the drop.

Solar-grade silicon samples (approximately 100 mg) were placed on the coated substrates and then heated under vacuum (10^{-6} mbar) to 800 °C for degassing. Then argon gas (6 N) was introduced with a flow rate of 0.7 L/min during heating to 1450 °C. The oxygen partial pressure in the furnace was measured by a zirconia sensor that was attached to the gas outlet and found to be about 10^{-19} atm upon melting, which is critical to avoid the formation of oxide layers on the silicon samples.

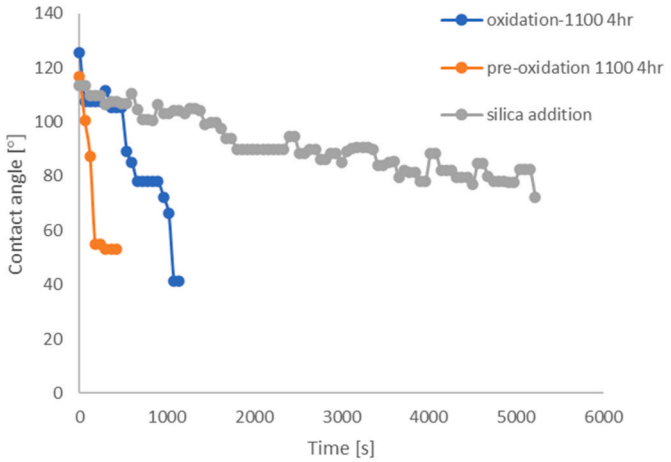

Fig. 1. Variation in the isothermal wetting behavior of three different coating techniques at 1723 K.

We investigated the wetting behavior at eight different mass concentrations of oxygen in the coating. The measurements were successfully replicated three times to assure reproducibility. Since wetting experiments are highly sensitive to the furnace conditions and operators [11], the run order of the in-situ experiments was randomized to eliminate the impact of any uncontrollable parameters.

Furthermore, a pilot-scale Si ingot was made in a coated silicon nitride crucible (Ø 25 cm). Oxygen was introduced to the coating by adding colloidal silica to the slurry. The coating layer was 150–200 μm and contained 10 wt% oxygen. The crucible was charged with 13.5 kg FBR/polysilicon feedstock and directional solidification was performed in a pilot-scale induction furnace: Crystalox DS-250. The ingot height after solidification was 10 cm without the seed layer. To investigate the coating degradation at different heights, samples were cut from the crucible after solidification for further characterization.

Electron Probe Microanalysis JXA-8500F was used to analyze the oxygen distribution in the coatings before and after the melting. The morphology and structure of the samples were studied using SEM Zeiss Ultra 55. To determine the chemical composition of the samples after melting, Raman mappings were performed using the WITec alpha300 R with a 532 nm laser. Raman spectra were obtained after 8 accumulations for 10 s from 50 to 1200 cm^{-1}.

3. Results and discussion

3.1. Wetting behavior

The contact angle development over time of the three proposed coating techniques is shown in Fig. 1. The silica addition to the coating shows a considerable improvement in the non-wettability behavior compared with the other two methods. The samples that were coated with pre-oxidized powder were wetted in a relatively short time. The wetting curve of the substrates that were treated by conventional oxidation matched those observed earlier in previous studies [16]. Based on these findings, the silica addition method was used for all the subsequent analysis.

Fig. 2 shows the effect of the coating's oxygen content on the contact angle development over time. The careful examination of the wetting curves indicates that the samples with 6–8 wt% oxygen in the coatings undergo the highest contact angles and the lowest wetting rates. All the

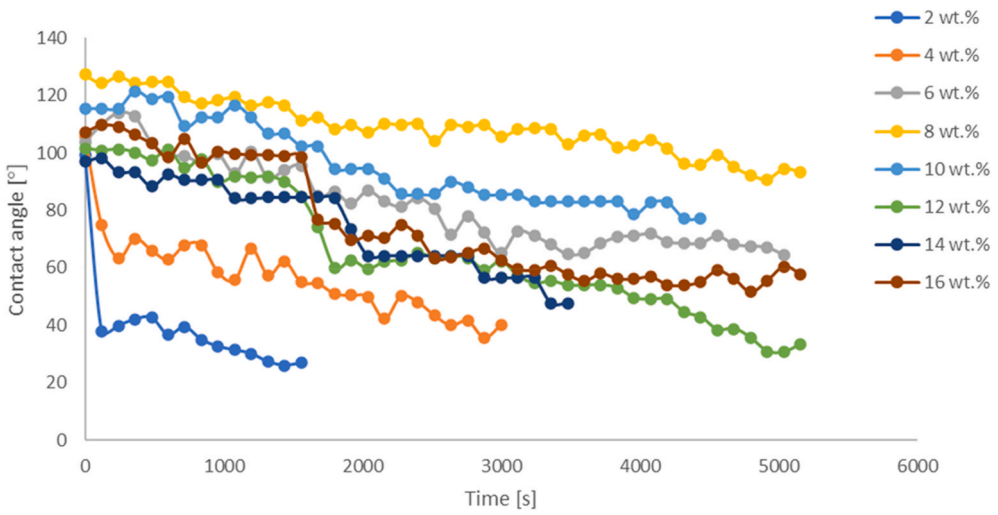

Fig. 2. The contact angle of silicon on Si_3N_4 substrates coated with different mixtures of Si_3N_4 and colloidal silica at 1723 K. The legend represents the initial oxygen mass concentration in the coating.

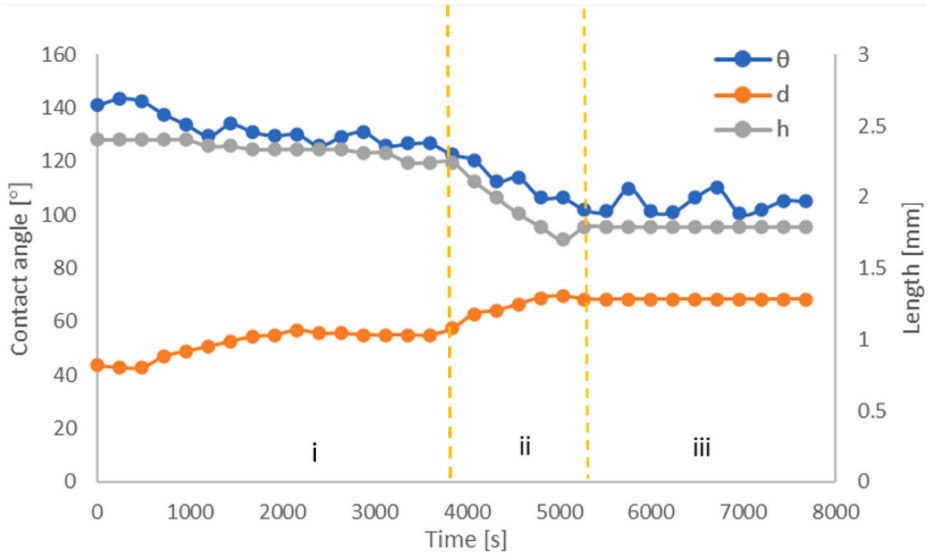

Fig. 3. Wetting curves for a sample that was coated with 8 wt.% oxygen content. Three parameters are measured: contact angle (θ), the height of the drop (h), and the diameter of the drop (d).

tested samples showed an isothermal transition in the wetting behavior that can be caused by a change in the chemical composition of the coating over time. Most studies define reactive wetting as a process where liquid and solid react and form an intermediate layer at the interface [18]. However, the continuous change in the contact angle that is combined with the change in the coating's chemical composition can be also considered as reactive wetting. To better describe the wetting stages, three geometrical parameters of the drop are measured over time. Fig. 3 shows the wetting curves of 8 wt% oxygen coated sample (see Supplementary Materials for all oxygen contents). Three major wetting stages are identified as follows: (i) a constant contact angle with no change in the height and the diameter of the drop (ii) a decrease in the contact angle and the drop height with an increase in the drop diameter, which represents a typical spreading situation, and (iii) a stable stage with no further advances in the wetting.

3.2. Coating degradation kinetics

Coating degradation refers to the change in the chemical composition of the coating as a result of the dissociation of its silica content when it interacts with the different components in the system during melting. In this work, we classified the degradation of the coating into three main regimes for sessile drop experiments and directional solidification as illustrated in Fig. 4 (a). The coating microstructure of the three regimes in sessile drop configuration: (i) under the droplet; liquid-solid system; (ii) at the triple line: solid-liquid-gas system; and (iii) away from the triple line: solid-gas system. These three regimes are indicated in Fig. 4 (c), (d) and (e), respectively. The obtained coating microstructures of the ingot growth experiment are included in Supplementary Materials (Fig. S3). Since each regime has its characteristic dominant reactions, the degradation rate calculations were performed separately for each one.

3.2.1. Liquid-solid system

This regime reflects the degradation of the coating under the droplet in sessile drop experiments and the degradation of the coating in contact with the bulk liquid in large scale crucibles. The degradation in this regime undergoes two major steps: First, the initial depletion occurs

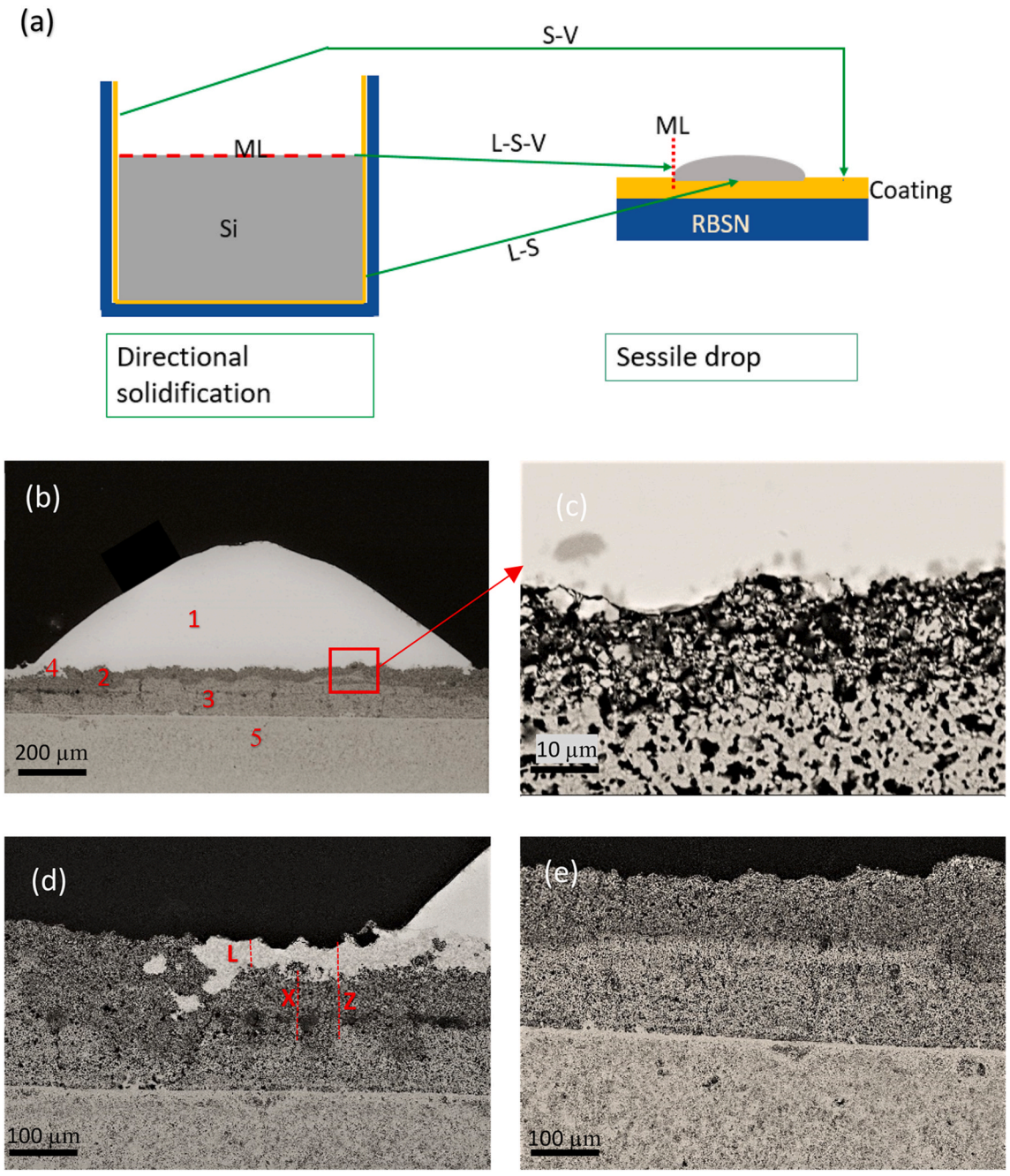

Fig. 4. (a) The three major regimes of the Si-coating system where S, L and V refer to solid, liquid and vapor phases respectively. (b) Typical drop -substrate configuration, (c) high magnification micrograph of coating's depletion under the droplet that shows the difference in the microstructure between the depleted and un-depleted coating. Coating microstructure at the triple line (d) and away from the triple line (gas-solid system) (e). 1: Si drop, 2: depleted coating, 3: un-depleted coating, 4: infiltrated coating, 5: Si_3N_4- substrate. L: infiltrated coating depth (m), X: eroded and un-infiltrated depth (distance between the infiltration front and silica-deoxidization front) Z: total eroded coating depth, (m).

Table 2
Possible reactions of silica decomposition at 1723 K.

Reaction	Formula	ΔG [J][a]	
Self-decomposition	$2SiO_2 \leftrightarrow 2SiO_g + O_2$	1.1593×10^5	(1)
Dissolution in liquid silicon	$SiO_2 + Si_l \leftrightarrow 2SiO_g$	-2.0882×10^5	(2)
Reduction by silicon nitride	$Si_3N_4 + 3SiO_2 \leftrightarrow 6SiO_g + 2N_2$	-2.6466×10^5	(3)

[a] Calculated by Factsage.

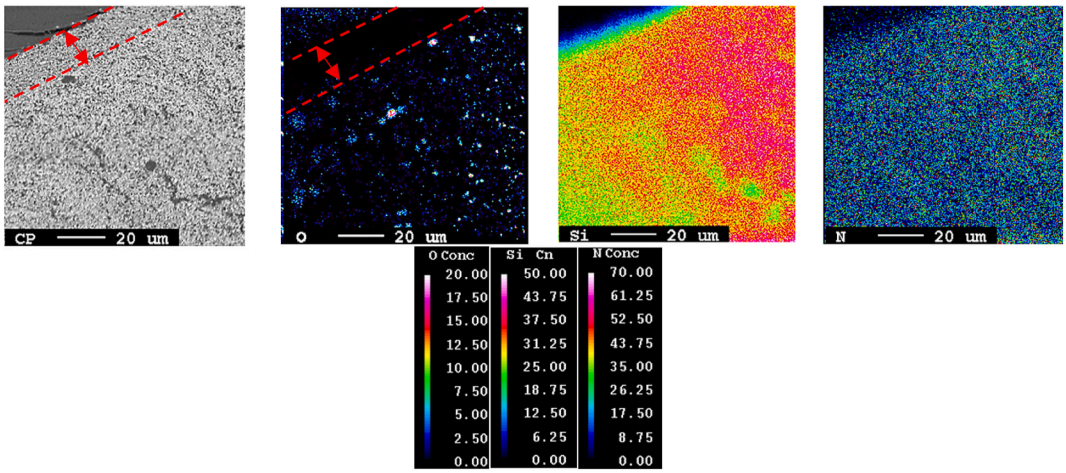

Fig. 5. An example of EPMA maps for a coated Si_3N_4 crucible after silicon melting. The red outlined area represents the depleted region. (For interpretation of the references to colour in this figure legend, the reader is referred to the Web version of this article.)

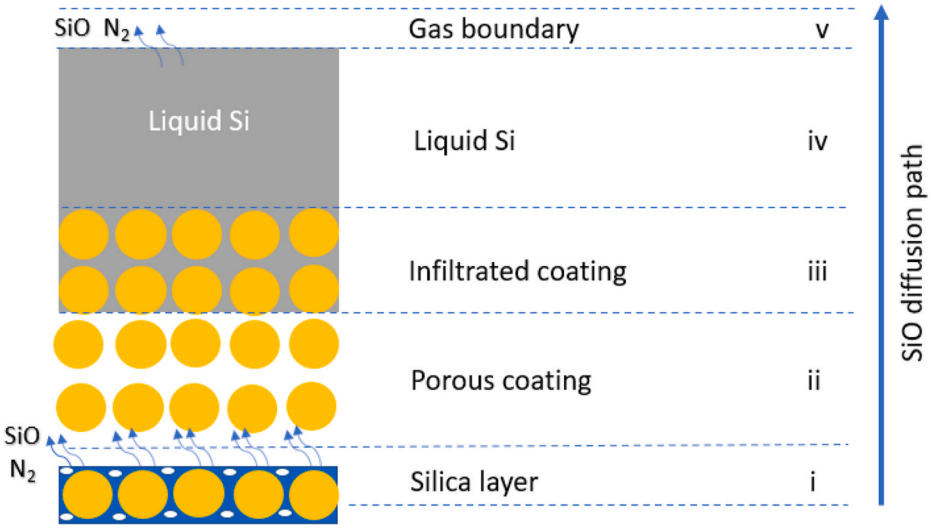

Fig. 6. The main steps of the SiO evacuation path under the droplet in the steady depletion stage (i–v). The orange circles correspond to the Si_3N_4 coating particles. The blue layer corresponds to the porous silica layer. (For interpretation of the references to colour in this figure legend, the reader is referred to the Web version of this article.)

when the underlying silica layer reacts with liquid silicon. This step is followed by a steady depletion where there is no direct contact between silica and the liquid phase.

3.2.1.1. Initial depletion. Table 2 lists all the possible reactions that lead to silica decomposition at 1723 K where the main product is SiO gas. Upon melting, silica dissolves into the liquid silicon by Reaction 2 as oxygen diffuses into liquid silicon and then evaporates as SiO to the boundary gas layer.

Huguet et al. [16] suggested that the limiting step of this reaction is the diffusion of oxygen in liquid silicon. Based on this, the depletion rate of the coating can be calculated by the equation below:

$$\frac{dZ}{dt} = \frac{D_l C_{Oi}^{eq}}{h_{drop}\, M_O} \tag{4}$$

Z is the depth of depleted coating which represents the vertical thickness of the coating that loses silica as illustrated in Fig. 4 (c) and evidenced by Fig. 5 that shows an example of the silica depletion, which was obtained by EPMA mapping. D_l is the diffusion coefficient of oxygen in liquid silicon (m^2/s). C_{Oi}^{eq} is the oxygen concentration of liquid silicon at equilibrium. h_{drop} is the height of the drop (m). M_O is the molar concentration of oxygen in the coating (mol/m^3). The transient period can be defined as the time required for the oxide layer that is in contact with molten silicon to dissolve, which also represents the duration of the direct contact between Si and SiO_2. As shown in Fig. 4 (b), the large distance between the infiltration front and depletion front (defined as X) suggests a fast-transient step. By integrating equation (1), the transient time can be calculated as follows:

$$t = \frac{\mathrm{f}\, h_{drop} M_O}{D_l C_{Oi}^{eq}} \tag{5}$$

f is the thickness of the silica layer that surrounds silicon nitride particles in the coating. The calculations of the transient period showed neglectable values compared with the overall experiment time. For example, the calculated transient time for 8 wt% sample was 93.4 s which represents 1.7% of the total experiment time.

3.2.1.2. Steady depletion. During the isothermal hold, the depletion of silica precedes the liquid infiltration as can be seen in Fig. 4(b) where there is a considerable distance between the infiltration front and the

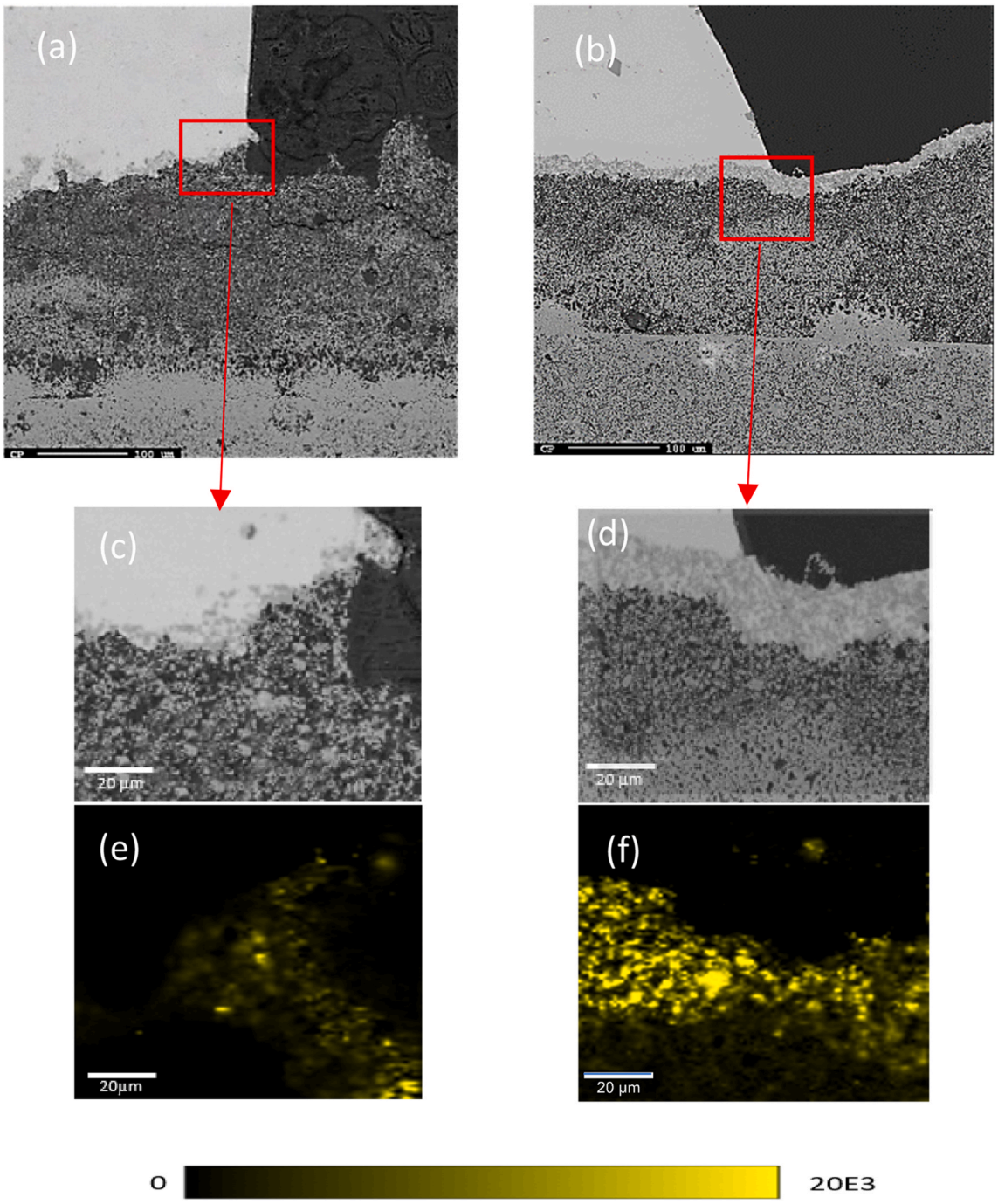

Fig. 7. Triple line region of two samples after sessile drop experiments at 1723 K and $t_h = 90$ min; (a) and (b) backscattered images of 8 and 16 wt % oxygen content respectively, (c) and (d) are the scanned areas by Raman, (e) and (f) are ß-Si_3N_4 mappings by Raman.

depletion front. This indicates that Reaction (2) is not valid any longer. The most favorable reactions among the list in Table 1, based on the Gibbs energy values, is the self-reduction reaction. To study the kinetics of this reaction, it is convenient to identify the main steps of the gas evacuation path under the droplet as illustrated in Fig. 6. The SiO evacuation was addressed since its partial pressure is three times higher than the nitrogen partial pressure. The time required for one SiO molecule to transfer from the reaction interface to the gas atmosphere is determined by the rate-limiting step. Full details of the model are provided in Appendix 1. According to the calculated diffusion rates at each step, the diffusion of oxygen in liquid silicon is considered as the rate-limiting step of the steady depletion. Hence, the coating depletion rate under the droplet is determined by the equations below:

$$\frac{dZ}{dt} \cong \frac{dL}{dt} = \frac{D_l C_{Oi}^{eq}}{(h_0 - L)M_O} \quad X_o << 0.08 \tag{6.a}$$

$$\frac{dZ}{dt} = \frac{D_l C_{Oi}^{eq}}{h_0 M_O} \quad X_o \geq 0.08 \tag{6.b}$$

L is infiltration depth (m). X_o is the mass concentration of oxygen in the coating. D_l is the diffusion coefficient of oxygen in silicon which equals $3.82 \times 10^{-8} m^2 s^{-1}$ [19] in liquid silicon and C_{Oi}^{eq} is the equilibrium concentration of oxygen in liquid silicon. More details can be found in the Appendix.

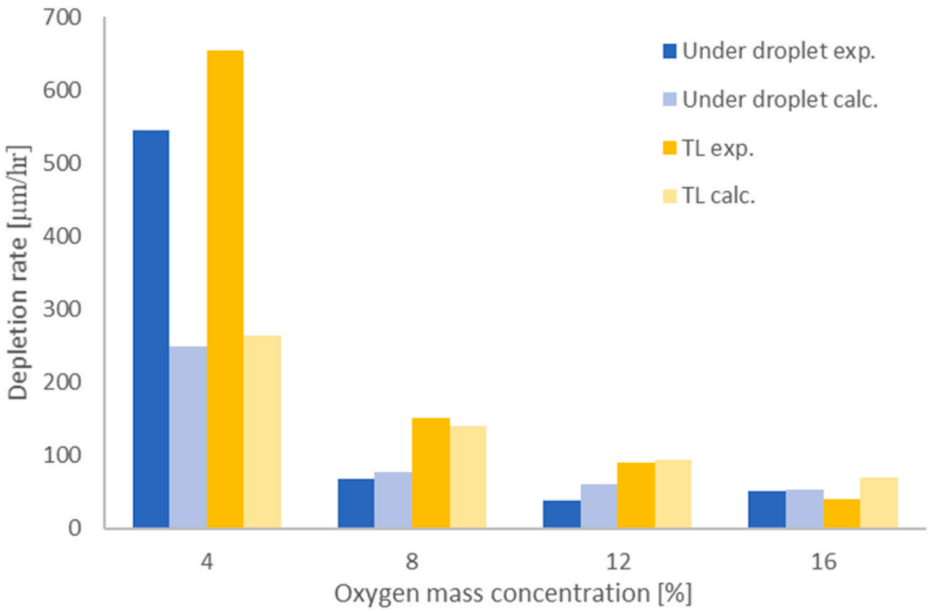

Fig. 8. The experimental and modelled results of coating depletion rates (µm/hr.) versus oxygen mass concentration in the coating: under the droplet and at the triple line.

3.2.2. Liquid-solid-gas system: at triple line

The triple line region is the three-phase contact line where liquid Si, coating and the gas atmosphere interact. We followed the same approach proposed in the previous section to model the depletion rate of the coating at the triple line. The degradation of the coating increases towards the triple line region as illustrated in Fig. 7(a) and (b). In this regime, the first three steps in the gas evacuation path are the same as in the liquid-solid system. Therefore, oxygen diffuses first through the silica layer, the porous coating, and the infiltrated coating (if it exists). Then it has two possibilities: diffusion directly into the gas boundary layer above the coating, or diffusion in the bulk liquid and then into the gas boundary. The mechanism is highly anisotropic as it varies with the distance from the triple line. Though, the depletion rate of the coating, that is located directly under the triple line, as shown in Fig. 7 (the red outlined areas) is limited by the diffusion of SiO in the silica layer and governed by the following equation:

$$\frac{dZ}{dt} = \frac{D^{E}_{SiO}\, P^{eq}_{SiO}}{RT\mathfrak{t} n_m} \tag{7}$$

$$D^{E}_{SiO} = \left(\frac{1}{D_b} + \frac{1}{D_K}\right)^{-1} \frac{\varepsilon}{\tau} \tag{7.1}$$

$$D^{E}_{SiO} = \left(\sqrt{\frac{2\pi M}{k_B T}} \left(\frac{8 P d_g^2}{3 k_B T} + \frac{3}{4 d_{SiO_2}}\right)\right)^{-1} \frac{\varepsilon}{\tau} \tag{7.2}$$

D^{E}_{SiO} is the effective diffusion coefficient of SiO in SiO_2 [20]. n_m is the molar density of SiO_2 (mol/m^3). t is the thickness of silica layer, which is calculated by the formula: ($t = r_0 - r_{XO}$), where r_{XO} is average pore radius of the coating at X_o. r_0 is the average pore radius of the Si_3N_4-coating without additions. The thickness of silica layer (at $X_o = 0.80$) is 1.5 µm P^{eq}_{SiO} is the equilibrium partial pressure of SiO at Si_3N_4–SiO_2 interface.. D_K is the Knudsen diffusion coefficient and D_b is the diffusion coefficient through the gas in the pores. d_{SiO_2} is the average pore diameter of the silica layer [21]. d_g is SiO molecular diameter ($0.26 \times 10^{-9} m$). ε is the porosity and τ is the tortuosity of the silica ($\tau = \varepsilon^{-0.5}$) [22]. M is the molecular weight of the diffusing species (SiO). k_B is the Boltzmann constant. The details of silica layer microstructure, the porosity and average pore diameter, are given in Supplementary Materials (Fig. S4).

3.2.3. Gas-solid system

This regime represents the coating regions that are in contact with the gas atmosphere and away from the liquid phase as displayed in Fig. 4 (d). It also represents the upper coated part of the crucibles (above the triple line). The SiO diffusion path consists of three main steps: (i) diffusion in the silica layer, (ii) diffusion in the porous coating, and (iii) diffusion in the gas boundary. The modelling of this process shows that the rate-limiting step is the diffusion in the silica layer. Hence, the coating degradation in this regime is inversely proportional to the thickness of the silica layer, which is mainly controlled by the oxygen mass concentration in the coating. Equation (4) describes the coating degradation in this regime and provides depletion rates that are similar to those calculated at the triple line since the limiting step is the same.

Fig. 8 shows the modelled and the experimental depletion rates versus the oxygen mass concentration in two main regimes. The proposed models fit well to the experimental data especially at $X_o \geq 0.08$. However, the experimental rates at lower oxygen contents are approximately two times higher than the calculated values. This difference might be explained by the dissolution of silicon nitride coating in the liquid that follows the depletion of SiO_2. Indeed, colloidal silica acts as a permanent binder in the coating and its dissociation alters the coating physical properties such as cohesion and porosity that can lead to the Si_3N_4 dissolution in Si. Therefore, this alteration in the coating microstructure suggests a considerable contribution of non-reactive infiltration, which is not involved in our model.

The depletion of coated crucibles can be calculated using the same approach as in the small-scale (See Table S1 in Supplementary Materials). Some additional issues, mainly related to some characteristics of the directional solidification, were considered in the calculations:

i. Melt contact time: as the melting front propagates from the top of the charged crucible and the solidification front propagates from the bottom, the duration of contact between liquid-Si and the coating varies with the height.
ii. Dissolution of the Si_3N_4-coating: coating's dissolution in the melt can also affect the experimental measurement of the eroded coating depths. However, in this case, its effect was neglectable since high melting and solidification rates were applied, and no significant dissolution was noticed at 10 wt.% oxygen content.

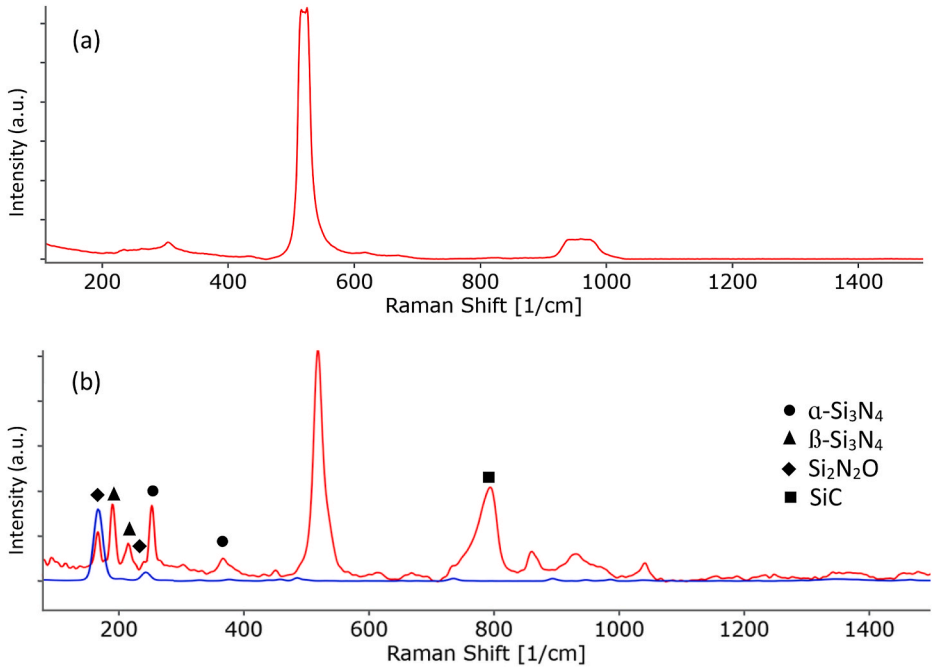

Fig. 9. Characteristic Raman spectra of the coating after the sessile drop experiment at 1723 K and $t_h = 90$. The red spectra are: (a) at the liquid front, (b) at the coating surface (in gas-solid regime). The blue is a reference for Si_2N_2O. The initial oxygen mass concentration in the sample is 8 wt%. (For interpretation of the references to colour in this figure legend, the reader is referred to the Web version of this article.)

Considering the coating that is in contact with liquid Si below the meniscus line, the rate-limiting step is the oxygen diffusion in the bulk liquid. The depletion depth in this regime varies with the height of the crucible. Therefore, the depletion rate increases towards the triple line because it has the longest holding time with the melt and minimum liquid path to the gas atmosphere. The depletion of the coating at the triple line, no contact with liquid, is higher than the previous regime and mainly controlled by the diffusion of the product gas in the silica layer. Similarly, in the gas-solid system, above the triple line, the depletion is limited to the thickness of the silica layer in the coating.

3.3. Effect of oxygen content on the infiltration kinetics

To understand why increasing the oxygen content in the coating does not reduce the wetting rates, we investigated the effect of oxygen content on the coating phase composition. Fig. 7 shows Raman mappings of two samples that contain different oxygen concentrations: 8 and 16 wt. %, respectively. As can be noticed, the depleted coating area in the sample with higher initial oxygen content, Fig. 7. (f), has a significantly higher content of ß-Si_3N_4. Since the same base coating powder is used for all samples, it seems that high oxygen content in the coating promotes the α-ß phase transformation during the wetting experiments. This finding also agrees with a previous study [23] that reported an increase of ß-Si_3N_4 content during sintering of oxidized silicon nitride samples. No studies have been found to examine the influence of ß-Si_3N_4 content on wettability. However, ß-Si_3N_4 particles are documented as more preferable nucleation sites for silicon, which implies low interfacial energy (γ_{sl}) between the particles and the silicon [24] and thereby a lower contact angle as suggested by Young's equation [25]:

$$\cos(\theta) = \frac{\gamma_{sv} - \gamma_{sl}}{\gamma_{lv}} \tag{8}$$

where γ is the interfacial tension between the liquid, solid and vapor phases. Therefore, the high oxygen concentration of the coating alters the microstructure via promoting α-ß phase transformation and hence increases the infiltration rate during melting. Though, other factors can contribute to the non-wetting properties at the optimal oxygen content as will be discussed below.

The infiltration in Si–Si_3N_4–SiO_2 is caused by the depletion of the oxygen in the coating as discussed earlier. This poses a question for the reason of the non-infiltration properties in the deoxidized coating such as at the optimal oxygen content and whether the kinetics of the depletion and the infiltration processes are similar. Based on our experimental findings, the coating depletion is found to lead to the liquid infiltration as depicted from the coated substrate microstructures in Fig. 4. Camel et al. [26] have reported the same observation in their study of the silicon-crucible interface. Thus, unlike the previous hypothesis in Ref. [16] that failed to predict the experimental infiltration rates, the two processes are not similar. Camel et al. [26] have claimed that the reprecipitation of silicon nitride at the Si–Si_3N_4 interface act as a barrier layer that hinders liquid penetration into the deoxidized coating. But the reprecipitation of silicon nitride is limited only to certain areas in the system, which cannot describe the overall behavior. Also, silicon nitride reprecipitation was not detected in our work. Fig. 9 depicts representative Raman spectra at the liquid interface and the coating surface. The peaks; 300, 520 and aboard peak at 950 cm^{-1} in Fig. 9 (a) correspond to amorphous silicon oxynitride (a-SiON) [27]. The intensity of these peaks increases at the liquid front. The a-SiON is also observed in the coating as shown in Fig. 9 (b) and its intensity increases towards the surface (Raman mappings of amorphous silicon oxynitride are included in Supplementary Materials). By comparing Raman Spectrum in Fig. 9 (b) with reference spectrum of Si_2N_2O [28,29], Si_2N_2O seems to exist in the coating. But, due to the high similarity between its crystal structure and ß-Si_3N_4 crystal structure, as can be seen in Fig. 9. (b), we relied only on the amorphous SiON mapping that indicates early stages of Si_2N_2O formation and/or disassociation. The silicon oxynitride forms at 1723 K in the coating by different reactions as listed below:

$$Si_3N_4 + CO \leftrightarrow Si_2N_2O + SiC + N_2 \quad \Delta G = -49588\ \text{J} \tag{9}$$

$$Si_3N_4 + SiO_2 \leftrightarrow 2Si_2N_2O \quad \Delta G = -81466.3\ \text{J} \tag{10}$$

$$2Si_l + \frac{1}{2}O_2 + N_2 \leftrightarrow Si_2N_2O \quad \Delta G = -9.3072 \times 10^4\ \text{J} \tag{11}$$

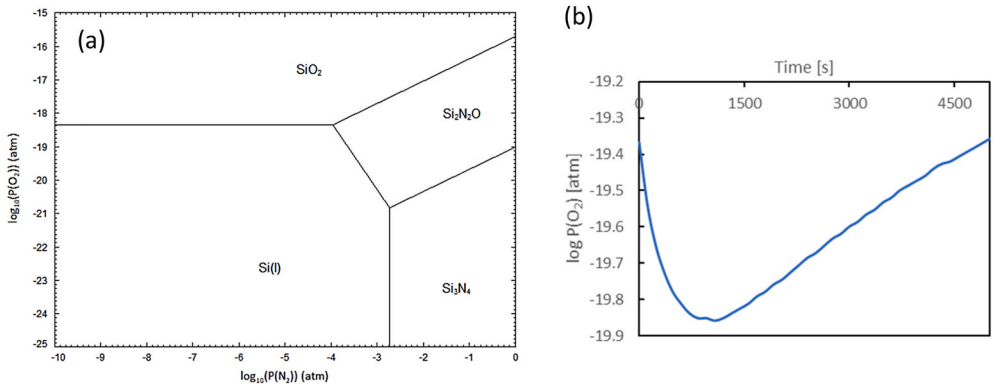

Fig. 10. (a) Predominance diagram for Si–O–N at 1723 K calculated by Factsage, (b) the oxygen evolution during the wetting experiment of a sample with 8 wt.% oxygen content in the coating at 1723 K.

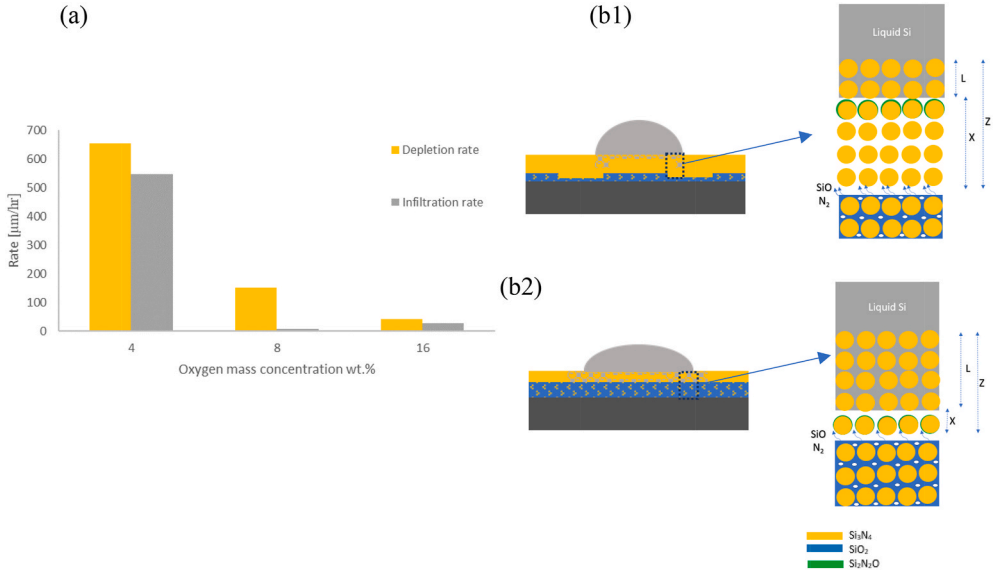

Fig. 11. (a) Experimental depletion and infiltration rates versus oxygen wt.% in the coating, (b) schematic drawing of the coating depletion and liquid infiltration mechanisms; (b1) at the optimal oxygen content (8 wt.%), (b2) at high oxygen content (16 wt.%).

Reaction (9) can be the main responsible for silicon oxynitride formation in the solid-gas regime since Raman analysis revealed the existence of SiC (see Fig. 9 (b)) at the coating surface. Furthermore, silicon oxynitride is the only intermediate compound in the SiO_2–Si_3N_4 system and can also form in the coating due to Reaction (10). However, Reaction (11) describes the formation of Si_2N_2O at the infiltration front as a result of saturation in Si by oxygen and nitrogen at the Si-coating interface, which is seen in Fig. 9 (a).

Previous studies [30–32] have also reported silicon oxynitride precipitation at the Si-coating interface, during directional solidification of Si. It is assumed that the interface is poorly wetted by the silicon [33]. Consequently, the presence of silicon oxynitride in the coating decreases its wettability and explains the liquid's resistance to penetrate the depleted coating. This indicates that the kinetics of liquid infiltration is mainly controlled by the stability of Si_2N_2O at the liquid-solid interface. To investigate the chemical stability of silicon oxynitrides, a predominance diagram of the Si–O–N system is constructed as shown in Fig. 10. The thermodynamic stability is ruled by the partial pressures of oxygen and nitrogen in the furnace, which are produced by the reduction of silica; Reaction (3). We measured the evolution of oxygen's partial pressure in the furnace during the wetting experiments as presented in Fig. 10(b). The partial pressure of oxygen increases from $10^{-19.6}$ to $10^{-19.3}$ atm during the isothermal hold due to the silica reduction. On the other hand, the equilibrium partial pressure of nitrogen gives a value of 6.0353×10^{-3} atm at 1723 K, according to the equilibrium constant of Reaction (3) (see Equation (A2) in Appendix). Thus, silicon oxynitride is most likely to form under these conditions. Indeed, the coating depletion process can be advantageous in reducing liquid infiltration as its gas products contribute to the formation of Si_2N_2O in the coating.

Finally, Fig. 11 (a) shows the experimental values of depletion and infiltration rates at different oxygen contents in the coating. As expected, the coating depletion rate is inversely proportional to the coating's oxygen content. Fig. 11 (b) schematically describes the infiltration mechanisms at two major oxygen values; 8 and 16 wt%, which are summarized as follows:

(i) At optimal oxygen content: silica depletion by Reaction (3) is considered as the major source of oxygen and nitrogen in the furnace, which maintains stable Si_2N_2O at the liquid-solid interface and the coating surfaces. Thus, due to the presence of poorly wetted Si_2N_2O compounds, infiltration and spreading are minimal in this case.

(ii) At high oxygen content: the high thickness of the silica layer in the coating results in a low depletion rate as the limiting step of this process is the diffusion of SiO in the silica layer. This negatively affects the Si_2N_2O stability due to the slow evolution rate of

oxygen and nitrogen in the furnace, which is not associated with a high decomposition rate of Si_2N_2O in liquid Si (see oxygen evolution plots in Supplementary Materials). The silicon oxynitride is mainly found at the liquid front.

4. Conclusions

A novel coating technique was developed for the non-oxide materials that can be used as reusable crucibles in Si-PV applications. This method eliminates the conventional pre-oxidation step, which is usually applied to the coated crucibles and limits the crucibles' lifetime by causing a severe degradation. The new coating technique showed better non-wetting properties during silicon melting compared with the conventional method.

The optimal oxygen content, 8 wt%, promises a notable high contact angle and a low wetting rate at minimal required silica addition to the coating. Increasing the oxygen content above the optimal value leads to higher infiltration and wetting rates. This may be due to the microstructure alteration caused by high oxygen concentration that lowers the α-ß phase transformation temperature.

The coating depletion rates during the melting process are modelled at different compositions of the coating to facilitate the adjustment of the coating parameters for silicon solidification processes. Based on the provided models, the coating thickness can be controlled to compensate for the predicted degradation of the coating during the Si casting process.

Moreover, it was revealed that the coating degradation, if controlled correctly, during melting can be advantageous for maintaining non-wetting conditions as it contributes to Si_2N_2O formation at the liquid front, which is poorly wetted by silicon. This explains the low infiltration rates of molten silicon in the degraded coating where the silica content is completely consumed.

Credit author statement

Rania Hendawi: Conceptualization, Methodology, Investigation, Formal analysis, Writing - Original Draft, Writing - Review & Editing. **Arjan Ciftja:** Resources, Writing - Review & Editing. **Lars Arnberg:** Conceptualization, Supervision, Validation, Writing - Review & Editing. **Marisa Di Sabatino:** Conceptualization, Supervision, Validation, Writing - Review & Editing. Funding acquisition, Project administration.

Declaration of competing interest

The authors declare that they have no known competing interests or personal relationships that could have appeared to influence the work reported in this paper.

Acknowledgements

This work was performed within the project Crucibles for Next Generation High Quality Silicon Solar Cells (CruGenSi), with contract number 268027 and funded by the Research Council of Norway and industry partners.

Appendix A. Supplementary data

Supplementary data to this article can be found online at https://doi.org/10.1016/j.solmat.2021.111190.

Appendix. Modelling of the depletion rate of Si_3N_4-coating

Here we derived the depletion rate for each step of the gas products transport path from the depletion reaction interface to the gas atmosphere.

i. Diffusion from SiO_2–Si_3N_4 interface through the SiO_2 layer:

Since silica encapsulates the silicon nitride particles, the product gases must diffuse first from the SiO_2–Si_3N_4 interface through the remaining silica layer that surrounds the silicon nitride particles. The depletion rate ($\frac{dZ}{dt}$) is obtained from the diffusion flux of SiO as follows:

$$J_{SiO} = \frac{D^E_{SiO} P^{eq}_{SiO}}{RT\text{f}} \tag{A1.1}$$

$$\frac{dZ}{dt} = \frac{D^E_{SiO}\, P^{eq}_{SiO}}{RT\text{f} n_m} \tag{A1.2}$$

J_{SiO} is the diffusion flux of SiO through SiO_2 layer ($mol.m^{-2}.\ s^{-1}$). If this step is the limiting step, then the concentration of SiO gas at the interface reaches the equilibrium and will be zero at the silica-pores interface. The equilibrium partial pressure of SiO at the reaction interface is calculated by the equilibrium constant of Reaction (3) as follows:

$$K = \exp\left(\frac{-\text{f}G^0}{RT}\right) = [P_{SiO}]^6 [P_{N_2}]^2 \tag{A2}$$

Based on the expression above, P_{SiO} at 1723 K is 1306 Pa.

ii. Diffusion in the porous coating:

This step represents the diffusion of SiO gas between the depletion front and the infiltration front which is defined as ($X = Z\text{-}L$) as illustrated in Fig. 5 c. Since X ≫ L, as revealed by Fig. 4(c), it can be assumed that L has a negligible effect on the depletion rate($L \approx 0$). Assuming that this step is the rate-liming step, the partial pressure of SiO at the depletion front will be equal to its equilibrium value with SiO_2. The depletion rate is calculated as follows:

$$\frac{dZ}{dt} = \frac{D_{SOE} P^{eq}_{SiO}}{RTM_O X} = \frac{D_{SOE} P^{eq}_{SiO}}{RTM_O (Z-L)},\ (L \approx 0) \tag{A3}$$

$$D_{SOE} = \left(\frac{1}{D_b} + \frac{1}{D_K}\right)^{-1} \frac{\varepsilon}{\tau} \tag{A4}$$

$$D_{SOE} = \left(\sqrt{\frac{2\pi M}{k_B T}} \left(\frac{8 P d_g^2}{3 k_B T} + \frac{3}{4d}\right)\right)^{-1} \frac{\varepsilon}{\tau} \tag{A5}$$

D_{SOE} is the effective diffusion coefficient in porous media [20]. D_K is the Knudsen diffusion coefficient and D_b is the diffusion coefficient through the gas in the pores, d is the average pore diameter of the coating. d_g is SiO molecular diameter ($0.26 \times 10^{-9} m$), ε is the porosity and τ is the tortuosity of the coating ($\tau = \varepsilon^{-0.5}$) [22]. M is the molecular weight of the diffusing species (SiO). k_B is the Boltzmann constant.

iii. Diffusion in the infiltrated coating:

If the oxygen diffusion in the infiltrated coating is the rate-limiting step, the oxygen concentration at the infiltration front will be equal to the equilibrium concentration in silicon and will reach zero at the coating-liquid interface. This assumption revokes the possibility of the coating depletion below the infiltration front as there is no driving force for it. This indicates that $X \approx 0$ and $Z = L$. The depletion rate is calculated by the equation below:

$$\frac{dZ}{dt} = \frac{\varepsilon D_l C_{Oi}^{eq}}{M_O Z \tau} \tag{A6}$$

D_l is the diffusion coefficient of oxygen in silicon which equals $3.82 \times 10^{-8} m^2 s^{-1}$ [19] in liquid silicon and C_{Oi}^{eq} is the equilibrium concentration of oxygen in liquid silicon which is given by the following equation [34]:

$$C_{Oi}^{eq} = .664 \exp\left(\frac{-2 \times 10^4}{T}\right) mol \Big/ cm^3 \tag{A7}$$

Since the liquid phase is saturated in the porous coating, the coating porosity and tortuosity are included in the depletion equation.

iv. Diffusion in the bulk liquid:

The depletion rate can be described by the following equations if the diffusion in the bulk silicon is the slowest step. The concentration of oxygen at the liquid front is C_{Oi}^{eq} and reaches zero at the liquid-gas interface. The depletion rate can be described as follows:

$$\frac{dZ}{dt} = \frac{D_l C_{Oi}^{eq}}{(h_0 - Z) M_O} \quad X_o << 0.08 \tag{A8.1}$$

$$\frac{dZ}{dt} = \frac{D_l C_{Oi}^{eq}}{h_0 M_O} \quad X_o \geq 0.08 \tag{A8.2}$$

The height of the drop decreases with time as a result of the liquid infiltration under the droplet. This effect can be neglected with high-oxygen content samples as ($h_{drop} >> L$) because of the minimal infiltration in the coating. However, at low oxygen contents in the coating where the infiltration and depletion rates are comparable, the decrease of height with time must be considered. In this case, for simplification purpose, the eroded and infiltrated depths can be assumed to be similar ($Z = L$).

v. Diffusion into the gas boundary:

At the liquid-gas interface, the dissolved oxygen in liquid Si reacts with silicon and evaporates as SiO gas into the argon gas atmosphere. If the diffusion of SiO gas in argon is the limiting step of silica depletion, the rate of depletion can be expressed as:

$$\frac{dZ}{dt} = \frac{D_{SiO} P_{SiO}^{eq}}{RTM_O r_{drop}} \tag{A9}$$

D_{SiO} is the diffusion coefficient of SiO in argon gas at 1723 K which is equal to $3.4 \times 10^{-4} m^2 s^{-1}$ [35].

It should be noted that the diffusion boundary thickness layer around the droplet is estimated to r_{drop} (drop radius) [36] because of the low Reynolds number (less than unity) at the given argon gas velocity ($u_{gas} = 0.67$ cm/s) where the volumetric argon flow at 273 K is 0.5 l/min and the chamber's diameter is 10 cm. The partial pressure of SiO at equilibrium at 1723 K is found to be 1653 pa according to Calberg's equation [34]:

$$\ln P_{SiO}(101325\ Pa) = \frac{-39,656}{T} + 18.9 \tag{A10}$$

In the case of SiO diffusion from the coating-gas interface, at the substrate surface, the gas boundary layer calculated as suggested elsewhere [14] gives a value of 14 mm at argon flowrate (Q_{Ar}) of 0.7 l/min.

We identified the rate-limiting step by calculating SiO diffusion rate in each step and comparing the resulting values with the experimental values.

References

[1] M.C. Schubert, F. Schindler, J. Benick, S. Riepe, P. Krenckel, A. Richter, R. Müller, B. Hammann, S. Nold, The potential of cast silicon, Sol. Energy Mater. Sol. Cell. 219 (2021) 110789.

[2] D. Hu, S. Yuan, L. He, H. Chen, Y. Wan, X. Yu, D. Yang, Higher quality mono-like cast silicon with induced grain boundaries, Sol. Energy Mater. Sol. Cell. 140 (2015) 121–125.

[3] N. Stoddard, B. Wu, I. Witting, M.C. Wagener, Y. Park, G.A. Rozgonyi, R. Clark, Casting single crystal silicon: novel defect profiles from BP solar's mono2 TM wafers, Solid State Phenom. 131–133 (2008) 1–8.

[4] Y. Lv, Y.F. Zhuang, W.J. Wang, W.W. Wei, J. Sheng, S. Zhang, W.Z. Shen, Towards high-efficiency industrial p-type mono-like Si PERC solar cells, Sol. Energy Mater. Sol. Cell. 204 (2020) 110202.

[5] C. Liu, D. Chen, Y. Chen, Y. Ling, Y. Zou, Y. Wang, J. Gong, Z. Feng, P.P. Altermatt, P.J. Verlinden, Industrial TOPCon solar cells on n-type quasi-mono Si wafers with efficiencies above 23%, Sol. Energy Mater. Sol. Cell. 215 (2020) 110690.

[6] H.C. Sio, S.P. Phang, A. Fell, H. Wang, P. Zheng, D.K. Chen, X. Zhang, T. Zhang, Q. Wang, H. Jin, D. Macdonald, The electrical properties of high performance multicrystalline silicon and mono-like silicon: material limitations and cell potential, Sol. Energy Mater. Sol. Cell. 201 (2019) 110059.

[7] V. Schneider, C. Reimann, J. Friedrich, G. Müller, Nitride bonded silicon nitride as a reusable crucible material for directional solidification of silicon, Cryst. Res. Technol. 51 (1) (2016) 74–86.

[8] C. Huguet, C. Dechamp, D. Camel, B. Drevet, N. Eustathopoulos, Study of interactions between silicon and coated graphite for application to photovoltaic silicon processing, J. Mater. Sci. 54 (17) (2019) 11546–11555.

[9] D. Camel, E. Cierniak, B. Drevet, R. Cabal, D. Ponthenier, N. Eustathopoulos, Directional solidification of photovoltaic silicon in re-useable graphite crucibles, Sol. Energy Mater. Sol. Cell. 215 (2020) 110637.

[10] A. Lan, C.E. Liu, H.L. Yang, H.T. Yu, I.T. Liu, H.P. Hsu, C.W. Lan, Silicon ingot casting using reusable silicon nitride crucibles made from diamond wire sawing kerf-loss silicon, J. Cryst. Growth 525 (2019) 125184.

[11] R. Hendawi, A. Ciftja, G. Stokkan, L. Arnberg, M. Di Sabatino, The effect of preliminary heat treatment on the durability of reaction bonded silicon nitride crucibles for solar cells applications, J. Cryst. Growth 542 (2020) 125670.

[12] K. Kazakyavichyus, D. Narbutene, E. Chasovskoi, A. Batura, V. Verevka, Thermal shock resistance of silicon nitride ceramics, Strength Mater. 20 (11) (1988) 1477–1480.

[13] B. Drevet, O. Pajani, N. Eustathopoulos, Wetting, infiltration and sticking phenomena in Si 3N 4 releasing coatings in the growth of photovoltaic silicon, Sol. Energy Mater. Sol. Cell. 94 (3) (2010) 425–431.

[14] B. Drevet, A. Selzer, V. Brizé, R. Voytovych, D. Camel, N. Eustathopoulos, Chemical stability of silicon nitride coatings used in the crystallization of photovoltaic silicon ingots. Part II: stability under argon flow, J. Eur. Ceram. Soc. 37 (1) (2017) 75–82.

[15] A. Selzer, V. Brizé, R. Voytovych, B. Drevet, D. Camel, N. Eustathopoulos, Chemical stability of silicon nitride coatings used in the crystallization of photovoltaic silicon ingots. Part I: stability in vacuum, J. Eur. Ceram. Soc. 37 (1) (2017) 69–74.

[16] C. Huguet, C. Dechamp, R. Voytovych, B. Drevet, D. Camel, N. Eustathopoulos, Initial stages of silicon–crucible interactions in crystallisation of solar grade silicon: kinetics of coating infiltration, Acta Mater. 76 (2014) 151–167.

[17] X. Gong, H. Du, X. Zhang, X. Hu, D. Zhang, Influence of the coating preparation method and of nanosilica addition on the bonding character of Si3N4 layer on a silica crucible, Ceram. Int. 40 (5) (2014) 7523–7529.

[18] G. Kumar, K.N. Prabhu, Review of non-reactive and reactive wetting of liquids on surfaces, Adv. Colloid Interface Sci. 133 (2) (2007) 61–89.

[19] Y. Itoh, T. Nozaki, Solubility and diffusion coefficient of oxygen in silicon, Jpn. J. Appl. Phys. 24 (3) (1985) 279–284. Part 1.

[20] M. Knudsen, The Kinetic Theory of Gases, 1934.

[21] A. Galukhin, D. Bolmatenkov, A. Emelianova, I. Zharov, G.Y. Gor, Porous structure of silica colloidal crystals, Langmuir 35 (6) (2019) 2230–2235.

[22] I.V. Thorat, D.E. Stephenson, N.A. Zacharias, K. Zaghib, J.N. Harb, D.R. Wheeler, Quantifying tortuosity in porous Li-ion battery materials, J. Power Sources 188 (2) (2009) 592–600.

[23] A. Qadir, Z. Fogarassy, Z.E. Horváth, K. Balazsi, C. Balazsi, Effect of the oxidization of Si3N4 powder on the microstructural and mechanical properties of hot isostatic pressed silicon nitride, Ceram. Int. 44 (12) (2018) 14601–14609.

[24] K.E. Ekstrøm, E. Undheim, G. Stokkan, L. Arnberg, M. di Sabatino, Beta-Si3N4 particles as nucleation sites in multicrystalline silicon, Acta Mater. 109 (2016) 267–274.

[25] N. Eustathopoulos, Dynamics of wetting in reactive metal/ceramic systems, Acta Mater. 46 (7) (1998) 2319–2327.

[26] D. Camel, B. Drevet, V. Brizé, F. Disdier, E. Cierniak, N. Eustathopoulos, The crucible/silicon interface in directional solidification of photovoltaic silicon, Acta Mater. 129 (2017) 415–427.

[27] C.K. Wong, H. Wong, J. Liu, A. Misiuk, Properties of silicon oxynitride films annealed under enhanced hydrostatic pressure, J. Electrochem. Soc. 158 (3) (2011) H322.

[28] T. Sekine, H. He, T. Kobayashi, K. Shibata, Sinoite (Si2N2O) shocked at pressures of 28 to 64 GPa, Am. Mineral. 91 (2–3) (2006) 463–466.

[29] C. Ma, J.R. Beckett, G.R. Rossman, Buseckite, (Fe,Zn,Mn)S, a new mineral from the Zakłodzie meteorite, Am. Mineral. 97 (7) (2012) 1226–1233.

[30] H. Matsuo, S. Hisamatsu, Y. Kangawa, K. Kakimoto, Distribution of light elements in multicrystalline silicon for solar cells grown by directional solidification, J. Electrochem. Soc. 156 (9) (2009) H711.

[31] H. Ono, T. Ishizuka, C. Kato, K. Arafune, Y. Ohshita, A. Ogura, Microscopic distributions of light elements and their precipitates in multicrystalline silicon for solar cells, Jpn. J. Appl. Phys. 49 (11) (2010) 110202.

[32] H. Ono, Y. Motoizumi, H. Kusunoki, K. Sato, T. Tachibana, A. Ogura, Formation of Si2N2O microcrystalline precipitates near the quartz crucible wall coated with silicon nitride in cast-grown silicon, APEX 6 (8) (2013), 081303.

[33] I. Brynjulfsen, A. Bakken, M. Tangstad, L. Arnberg, Influence of oxidation on the wetting behavior of liquid silicon on Si3N4-coated substrates, J. Cryst. Growth 312 (16) (2010) 2404–2410.

[34] T. Carlberg, Calculated solubilities of oxygen in liquid and solid silicon, J. Electrochem. Soc. 133 (9) (2019) 1940–1942.

[35] D.E. Bornside, R.A. Brown, T. Fujiwara, H. Fujiwara, T. Kubo, The effects of gas-phase convection on carbon contamination of czochralski-grown silicon, J. Electrochem. Soc. 142 (8) (1995) 2790–2804.

[36] D.J. Tritton, Low and high Reynolds numbers, in: D.J. Tritton (Ed.), Physical Fluid Dynamics, Springer Netherlands, Dordrecht, 1977, pp. 81–87.